

# Interplay between one-particle and collective degrees of freedom in nuclei

Ikuko Hamamoto\*

*Riken Nishina Center, Wako, Saitama 351-0198, Japan*

*Division of Mathematical Physics, Lund Institute of Technology at the University of Lund, Lund, Sweden*

PACS REF: 21.10.Gv, 21.10.Pc, 21.10.Re, 21.60.Ev, 23.20.-g, 23.20.Lv

## Abstract

Some developments of nuclear-structure physics uniquely related to Copenhagen School are sketched based on theoretical considerations versus experimental findings and one-particle versus collective aspects. Based on my personal overview I pick up the following topics; (1) Study of vibration in terms of particle-vibration coupling; (2) One-particle motion in deformed and rotating potentials, and yrast spectroscopy in high-spin physics; (3) Triaxial shape in nuclei: wobbling motion and chiral bands; (4) Nuclear structure of drip line nuclei: in particular, shell-structure (or magic numbers) change and spherical or deformed halo phenomena; (5) shell structure in oblate deformation.

## 1. Introduction

I came to Copenhagen in September, 1967, holding one-year's fellowship from the Nishina Foundation in Japan. It was my first visit to foreign institutes, where I had to understand physics discussed in English. Indeed, it took several years for me to understand some physics which I heard in English. Everything was new and interesting to me, but among others, I remember clearly "experimental meeting at NBI (= Niels Bohr Institute)" at 11 o'clock on Monday morning, in which I learned how to talk with and study from experimentalists. New experimental data presented by experimentalists coming from all over the world were of course exciting, however, it was my strong impression that people were more carefully watching the questions and reactions by Aage Bohr and Ben Mottelson to those presentations. In the sixties at NBI we could meet physicists from both West (USA, Canada, Europe, Australia, etc.) and East (Soviet Union, East Europe, China, etc.), and we became good friends for life after we spent our younger days together.

My stay in Copenhagen, which at the beginning I intended for one year, became for three years. Though I once left Copenhagen in the summer of 1970, I came back to Europe already in 1971 and to Copenhagen in 1973. Since 1971 I helped the completion of Bohr and Mottelson's book, NUCLEAR STRUCTURE vol. II, which was finally published in 1975. The book is not at all just a textbook, but the entire volume is a big article, which is full of their original ideas and deeply-going understanding of physics. During those years I learned an enormous amount of physics from Bohr and Mottelson especially because I could directly talk with them and ask questions to them almost whenever I wanted. It was the exclusively precious and happy time and days in my life as a physicist, which I never forget, and I want to express my heartfelt thanks

to Aage and Ben.

In the present article I write my personal overview of five topics that have been centrally placed in the field of nuclear-structure physics in respective decades. Those topics perhaps except for the most recently developed drip-line physics have been developed in the way either strictly followed from the ideas of Bohr and Mottelson or strongly influenced by their way of thinking physics, and the topics are those, the study of which I myself have also eagerly worked in. In Sec. II particle-vibration coupling, in Sec. III one-particle motion in deformed and rotating potentials, and yrast spectroscopy in high-spin physics, in Sec. IV triaxial shape of nuclei, in Sec. V nuclear structure as neutron-drip-line approaches, and in Sec. VI nuclear shell-structure in oblate deformation are presented, while conclusions and discussions are given in Sec. VII.

## 2. Particle-vibration coupling

In the self-consistent system such as nuclei one-particle motion and collective phenomena are strongly related. Elementary modes of excitations may be associated with excitations of individual particles or they may represent collective vibrations of the density, shape, or some other parameter that characterizes the equilibrium configuration. The vibrational motion in nuclei is so profoundly affected by the shell structure of one-particle motion that it presents an excellent example of the interweaving of one-particle and collective degrees of freedom [1].

In the nuclear system the possibility of collective shape oscillations is strongly suggested by the fact that the ground states of some nuclei are described by densities and mean fields that are spherical while others are deformed. Consequently, one might expect to find intermediate situations in which the shape undergoes rather large fluctuations away from the equilibrium shape. In addition to the modes which have classical analogs, in the nuclear spectra vibrational modes unique in a quantal system, such as those involving charge exchange or excitation of the nucleonic spins or oscillations in the pair field, are known and studied.

In the following of this section we take shape oscillations as an example of particle-vibration coupling, because experimental study of various properties of them has been carried out for years and the resulting data are accumulated. The density variations associated with the vibrational motion make corresponding variations in the average potential. The distortion of the average potential gives a coupling between the degrees of freedom of the vibration

\*e-mail: [Ikuko.Hamamoto@MATFYS.LTH.SE](mailto:Ikuko.Hamamoto@MATFYS.LTH.SE)

and individual particles [1],

$$\delta V = -k_\lambda(r) \sum_{\mu} Y_{\lambda\mu}^*(\theta, \phi) \alpha_{\lambda\mu} \quad (1)$$

where

$$k_\lambda(r) = R_0 \frac{\partial V(r)}{\partial r} \quad \text{or} \quad r \frac{\partial V(r)}{\partial r} \quad (2)$$

where  $R_0$  expresses the radius of the average static potential,  $V(r)$ , for which we use the form of Woods-Saxon potential. Either radial form on the r.h.s. of (2) that is used in various publications gives nearly the same numerical results because the quantity  $\partial V(r)/\partial r$  is concentrated on the nuclear surface, though the first form can be more reasonable.

One may consider a number of effects which arise from the coupling: For example, the renormalization of the properties of both particles and vibrations, or a self-consistent description of the vibrational motion itself in terms of one-particle degree of freedom, or the effect of the exclusion principle between the degrees of freedom of particles and those involved in the vibrational modes, as well as the orthogonality of different modes. In particular, in the case of the coupling being weak enough to be treated by perturbation, one can systematically calculate those various effects, and the comparison between the calculated quantities and the observed ones provides a quantitative information on the validity of our understanding of the structure of the basic particle-vibration coupling.

Particle-vibration coupling in low-lying quadrupole vibrations is often too strong to be quantitatively treated by perturbation. In contrast, low-lying octupole vibrations provide the data, by which our understanding can be quantitatively tested. A beautiful example is related to the octupole vibration of the doubly magic nucleus,  $^{208}_{82}\text{Pb}_{126}$ . There are many kinds of data on octupole vibrations in neighboring nuclei of  $^{208}\text{Pb}$  [2], which were nicely interpreted in terms of the particle-vibration coupling. In the following we take the septuplet of the octupole vibration,  $[(h_{9/2} 3^-)_I, I^\pi = 3/2^+, \dots, 15/2^+]$ , observed in  $^{209}_{83}\text{Bi}_{126}$ , as a beautiful example of the particle-vibration coupling. In Fig. 1 observed low-lying energy spectra of  $^{208}_{82}\text{Pb}_{126}$  and  $^{209}_{83}\text{Bi}_{126}$  that are relevant to the present discussion are shown.

In the calculations of respective observed quantities shown in the following the contributions only in the lowest-order perturbation were taken into account. However, it is important to note that all contributions in the lowest order are included when differential equations appropriate for respective contributions were numerically integrated instead of expanding the wave-functions in terms of a given finite basis.

A number of beautiful experiments on many faces of the septuplet members have been carried out especially during the sixties and the seventies, such as energies, decay scheme and octupole strength of respective members, one-nucleon transfer reaction cross section to populate some members. The properties of the octupole vibration itself in  $^{208}\text{Pb}$  such as the transition density, quadrupole moment, and double-phonon states were also explored. Observed data in connection with this octupole vibration could be in almost all cases treated by perturbation and gave a firm

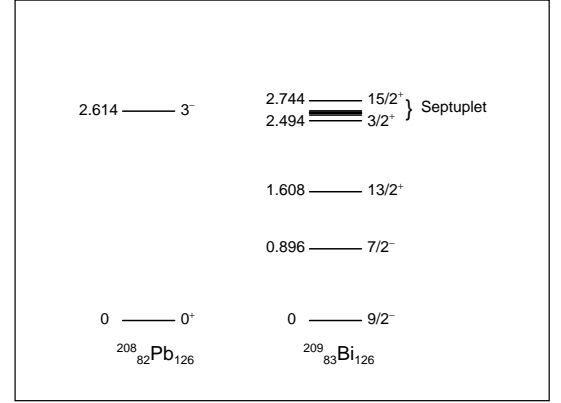


Fig. 1: Observed low-lying energy spectra of  $^{208}_{82}\text{Pb}_{126}$  and  $^{209}_{83}\text{Bi}_{126}$  that are relevant to the present discussion. Excitation energies are expressed in MeV.

support for our understanding of the shape (surface) oscillation and the related particle-vibration coupling. The detailed comparison between experimental and calculated results can be found in available publications. See, for example, [2]. Therefore, in the following I show only two examples; (i) energy shifts and the decay scheme of the septuplet members of  $^{209}\text{Bi}$  and (ii) the radial transition density of the octupole vibration of  $^{208}\text{Pb}$ .

Parameters used as an input in the numerical calculations are the two observed quantities in  $^{208}\text{Pb}$ ; the observed vibrational energy, 2.614 MeV, and the observed vibrational strength,  $B(E3) = 32 B_W(E3)$ , which is used to obtain the matrix element of  $\langle n_3 = 1 | \alpha_3 | n_3 = 0 \rangle$ . The value of  $32 B_W(E3)$  was taken from Coulomb excitation experiments [3, 4, 5].

In Table 1 calculated energy shifts (in the 2nd-order perturbation of the particle-vibration coupling) and the decay scheme (in the 1st-order perturbation of the particle-vibration coupling) of the septuplet members in  $^{209}\text{Bi}$  are compared with experimental ones. The observed energy splitting of the septuplet is 250 keV compared with 350 keV of the calculated one. We note a remarkable agreement between the calculated and experimental decay schemes, in particular, six  $B(E1)$ -values obtained using  $[e_{eff}^p(E1)]^2 = 0.14 e^2$ , while it is known to be extremely difficult to predict  $B(E1)$  values in strongly-hindered low-energy E1 transitions in nuclei. This agreement may be used for supporting our basic understanding of the present particle-vibration coupling and the surface vibration. In addition, the obtained value of  $e_{eff}^p(E1)$  agrees approximately with the value [1] estimated by taking into account the reduction coming from both the center of mass motion and the presence of the isovector giant dipole resonance.

In Fig. 2 the calculated radial transition density (in the 1st-order perturbation of the particle-vibration coupling) of the  $3^-$  state of  $^{208}\text{Pb}$  [7] is compared with those obtained from electron inelastic scatterings. The large

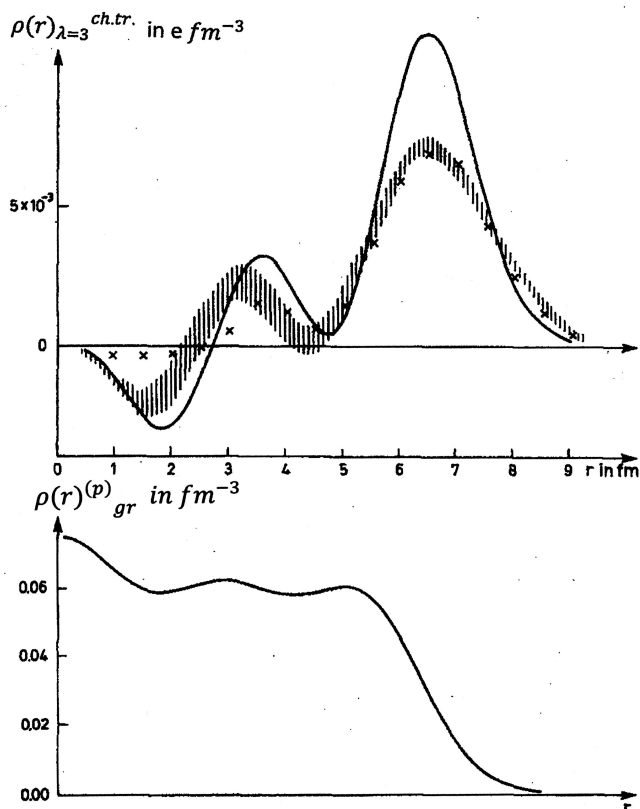


Fig. 2: The upper part expresses the radial transition charge density of the  $3^-$  state at 2.614 MeV in  $^{208}\text{Pb}$ . The solid line shows the calculated value [7], while for the experimental values the dashed band was taken from Ref. [8] and the crosspoints were from Ref. [9]. The lower part of the figure denotes the calculated charge density of the ground state of  $^{208}\text{Pb}$ . The scale of the x-axis in the lower part is the same as the one in the upper part. The figure is adapted from Fig. 1 of Ref. [7].

peak around the surface can be understood as a feature of the shape oscillation. The position of the first minimum around 5 fm coincides closely with the  $r$ -value where the ground-state density reaches the maximum, noting that the radial transition density is approximately proportional to the radial derivative of the static density. The structure of the two small peaks inside the nucleus depends on the microscopic shell-structure of the octupole vibration in addition to the general quantum-mechanical oscillatory structure of the static density.

Another example in somewhat lighter-mass region, which exhibits a very similar coupling between particles and an octupole vibration, was reported in 1982 [10]. The septuplet members in  $^{147}\text{Gd}_{83}$ ,  $(f_{7/2} 3^-)_{I^+}$  with  $I = 1/2, \dots, 13/2$ , in which the octupole vibration  $3^-$  of  $^{146}\text{Gd}$  at  $E_{ex} = 1.579$  MeV with  $B(E3) = 37 B_W(E3)$  was coupled to the 83rd odd-neutron in the  $f_{7/2}$  orbit, were identified except the  $I^\pi = 5/2^+$  member. Due to the dominance of the proton  $(h_{11/2} d_{5/2}^{-1})_{3^-}$  component in the  $3^-$  state, not all properties of the septuplet members could be analyzed by perturbation. However, it is unique in the case of the octupole vibration of  $^{146}\text{Gd}$  that the two-octupole-phonon angular-momentum-stretched state,  $[(\nu f_{7/2})(3^-)^2]_{19/2^+}$ , in  $^{147}\text{Gd}$  was experimentally identified and the pretty strong anharmonicity in both the energy and the E3 transition rate was subsequently analyzed [11].

### 3. One-particle motion in deformed and rotating potentials, and yrast spectroscopy in high-spin physics

The very basic description of nuclear many-body systems is the (self-consistent) mean-field approximation to the many-body problem. In particular, shape is the property of mean field. The ground states of some nuclei are described by densities and mean fields that are spherical, while others are deformed. In Fig. 3 the even-even nuclei, of which the ground state is observed to be deformed, are shown. The deformation results from one-particle shell-structure, namely bunching of one-particle levels, in contrast to the prediction of the liquid-drop model. For the nucleus as a quantum many-body system the presence of deformation is a necessary condition for the occurrence of collective rotation, and the symmetry of the deformation determines the structure of rotation. The most important deformation around the ground states of nuclei is the axially-symmetric quadrupole deformation corresponding to a spheroidal shape (cigar or pancake). Axially-symmetric nuclei cannot perform a collective rotation about the symmetry axis.

If some nuclei show deformation with a given symmetry it is simplest and most convenient to start with the mean field, which has the same symmetry. One-particle motion in quadrupole-deformed potentials was solved in the fifties almost at the same time by three groups [12, 13, 14]. Among them, "Nilsson model" [12] has been used by many people in the analysis of data, presumably because the application of the Nilsson model using modified oscillator potentials to actual nuclei was easiest and very practical. The spectrum of one-particle orbits as a function of deformation, so-called "Nilsson diagram", has played an invaluable role in the study of deformed nuclei. (In the present article the word, "Nilsson diagram", is used for the diagrams of one-particle energies as a function of quadrupole deformation using general one-body potentials such as Woods-Saxon or HF potentials, and not only for the diagram drawn by using modified oscillator potentials.) Nilsson diagrams have been extremely useful for analyzing the data on deformed nuclei. This is mainly because the major part of the  $(Y_{20}^* \cdot Y_{20})$  channel of the two-body quadrupole-quadrupole interaction is absorbed into the mean field. Consequently, the picture of one-particle motion in the deformed potential works for deformed nuclei much better than that of one-particle motion in spherical potentials for spherical nuclei. For example, see the successful quantitative analysis of various kinds of experimental data of well-deformed (especially odd-A) nuclei such as  $^{25}\text{Mg}$ ,  $^{25}\text{Al}$ ,  $^{159}\text{Tb}$ ,  $^{169}\text{Tm}$ ,  $^{175}\text{Yb}$ ,  $^{175}\text{Lu}$ ,  $^{177}\text{Lu}$ ,  $^{177}\text{Hf}$ ,  $^{235}\text{U}$ ,  $^{237}\text{Np}$ ,  $^{239}\text{Pu}$  presented in Ref. [1].

The field of nuclear high-spin physics was activated by the observation of the "back-bending" phenomena [15], which was the first band-crossing (between the ground-band and the S-band) along the yrast line in well-deformed collectively-rotating nuclei. During the seventies the possibility of studying nuclei with very large angular-momentum was opened up, thanks to the facilities of accelerating heavy-ions. Collisions between two heavy nuclei could produce meta-stable compound systems with large angular-momenta. Indeed, in heavy-ion collisions in the

late seventies it was possible to produce compound nuclei with angular momentum all the way up to the limit set by the fission instability. The maximum value of angular momentum which nuclei can accommodate is the order of  $100\hbar$  for nuclei with  $A \approx 130$  [16]. The study of rapidly rotating nuclei provided the opportunity for exploring new aspects of nuclear dynamics [17, 18, 19, 20].

When the angular momentum is accommodated by a quantal system such as a nucleus, one recognizes that there are two fundamental ways of building the angular momentum [21]. The first one is collective rotation in the presence of a significant amount of deformation, while the second one is to build the angular momentum by spin alignments of individual particles when the angular momentum is directed along an axis of symmetry of the nucleus. In actual nuclei we encounter situations in which the increment of angular momentum is achieved partly by increasing the frequency of collective rotation and partly by rearranging the occupation of one-particle orbits (namely, by increasing the particle alignments). In fact, the collective rotational spectra together with the crossing of the ground band with the S-band are characteristic of this kind of situation.

Special interest in nuclear high-spin states attaches to the region in the neighborhood of the yrast line representing the lowest energy for a given angular-momentum. In this yrast region the nucleus is cold in the sense that almost the entire excitation energy of the nucleus is consumed in generating the angular momentum. Therefore, the structure in the yrast region is ordered with simple excitation modes, and the study of those may be expected to give important nuclear-structure information on how the nucleus responds to the large centrifugal forces associated with rotation. The path that the yrast line of actual nuclei will follow in deformation space with increasing angular-momentum will result from the competition between the macroscopic centrifugal distortion effect and the quantal effects associated with shell-structure.

In the yrast spectroscopy of medium-heavy nuclei an important role has been played by particles in high-j orbits, such as  $1g_{9/2^-}$ ,  $1h_{11/2^-}$ ,  $1i_{13/2^-}$  and  $1j_{15/2^-}$ -orbits. This is because the parity of high-j orbits is different from that of other one-particle orbits in respective major shells, therefore, both in quadrupole deformation and under rotation particles in high-j orbits do not mix with those in neighboring orbits. That means, the wave functions of particles in high-j orbits have less ambiguity. Furthermore, as soon as rotation sets in, particles in high-j orbits start to align due to the particularly large Coriolis coupling, while particles in neighboring other orbits still contribute to collective rotation. Consequently, the states consisting of high-j-shell configurations easily appear in the neighborhood of the yrast line. A typical example is that the intrinsic structure of the S-band contains a large alignment coming from the aligned two quasiparticles in the relevant high-j orbit, in contrast to the absence of such alignment in the ground band, at the angular momentum of the band crossing.

The basis for the analysis of shell-structure effects on nuclear high-spin states is the study of one-particle motion in rotating potentials. The importance of understanding the physics in the yrast region, especially in terms of one-particle motion in rotating potentials, was repeatedly

emphasized by Bohr and Mottelson during the seventies. The cranking model is easily treated and the rotational frequency appears as an explicit parameter. Indeed, the major part of the analysis of nuclear high-spin phenomena has been carried out in terms of cranking models of various types. In particular, the so-called Routhian diagram, namely the diagram plotting one quasiparticle energies in the rotating frame as a function of cranking frequency, played for years a central role in the analysis of nuclear high-spin data. I remember that around the middle of the seventies Aage Bohr was repeating to say to us working at the Niels Bohr Institute that one should draw and study the Routhian diagram for fixed deformation and pairing parameters. (At that time I stupidly thought that such simplified Routhian diagrams might be qualitatively excellent for getting ideas and ways of understanding physics, but they would hardly be useful for practical numerical applications.) In this connection, I later realized that, for example, without plotting such Routhian diagrams it would have been indeed difficult to notice the fact that the interaction strength between the ground band and the S-band, namely the sharpness of backbending phenomena, is an oscillating function of the degree of high-j-shell filling [22]. The extended study with numerical works using realistic configuration spaces was eventually carried out by R. Bengtsson and S. Frauendorf [23], and the Routhian diagrams of such a simple type turned out to be extremely useful and have been successfully used in the analysis of high-spin data for the following years.

However, one should keep in mind that the uniform rotation of a system, which is a basic assumption of the cranking model, may become a poor approximation under certain circumstances, because the presence of fluctuations in the collective rotational frequency is recognized if one treats more reasonably the exchange of angular momentum between individual particles and the potential produced by the rest of the system [24]. An example outside the applicability of the cranking model in its simplest form is the description of the crossings of the bands with a large difference of spin alignments, irrespective of whether the parameters in the model are chosen self-consistently or not. The inapplicability comes from the fact that a mixing of the two bands for a given rotational frequency is basically considered in the cranking model, while the two bands should interact for a given angular momentum [25].

The experimental front of high-spin physics made a tremendous progress in the decades after the observation of "back-bending", especially due to the development of multi-gamma-ray detectors, which had a resolution of orders greater than that of the last generation, and  $4\pi$  or  $8\pi$  spectrometers; NORDBALL and TESSA  $\rightarrow$  EUROGAM and GASP  $\rightarrow$  EUROBALL and GAMMASPHERE.

New frontiers were opened in the nuclear high-spin physics, when the superdeformed band in  $^{152}_{66}\text{Dy}_{86}$  was reported [26] by finally observing gamma-ray spectra of discrete transitions in the decay sequence of the superdeformed band of  $^{152}\text{Dy}$  extending to  $I \approx 60\hbar$ , thanks to the development of detectors. The observation of the discrete gamma-rays could directly and clearly show the presence of the superdeformed band, compared with the information extracted previously from the painstaking analysis of complicated continuum gamma-rays. It is noted that the

largest angular momentum, which was reported in discrete line studies before the discovery of the superdeformed band, was only  $46 \hbar$ . Because of the large moment of inertia of superdeformed nuclei, the large angular-momentum needed for the study of such systems does not necessarily mean large rotational frequencies. Consequently, the unique behavior of particles in high- $j$  orbits could largely remain also in the analysis of superdeformed bands. The shape of superdeformation in nuclei, where the axis ratio of the prolate-deformed shape is approximately 2:1, was known already in the sixties as (low-spin) fission isomers in actinide nuclei [27] and was interpreted as the result of the shell-structure which appears first for much larger quadrupole-deformation ( $\beta \approx 0.6$  in medium-heavy nuclei) than the one known in nuclear ground states. In subsequent years the observation of super- or highly-deformed bands was reported also in other mass region than  $A=150$ , such as  $A=130$  [28] and 190 [29], though the relevant shape was not always close to 2:1.

Before 1975 the view might have been accepted that there were nuclei that were statically deformed and they were located far away from closed shells, while there were nuclei that were spherical and they were located in the neighborhood of closed-shell regions, though in some nuclei located on the border of spherical and deformed nuclei the simultaneous presence of the low-lying states with spherical and deformed shapes was already recognized. Thanks to the marvelous development of experimental techniques in high-spin physics, collective rotational bands were found at the excitation energy of several MeV also in some nuclei such as  $^{82}\text{Pb}$ ,  $^{50}\text{Sn}$  and  $^{20}\text{Ca}$  isotopes [30], which are at least semi-magic and were supposed to be spherical. While it has been known that for a given nucleus Hartree-Fock calculations often predicted local energy-minima at several different deformations, the possible presence of such several shapes in a given nucleus has been indeed confirmed thanks to the modern experimental technique.

In the present special issue of *Physica Scripta* I expect a number of contributions by specialists in the field of high-spin physics. Therefore, to those contributions I would leave to show a tremendous amount of beautiful results obtained from all detailed numerical works in comparison with exciting and impressive experimental data.

#### 4. Triaxial shape in nuclei

Theoretically the existence of nuclear deformation other than axially-symmetric deformation was predicted, and it has been a great challenge to find the predicted axially-asymmetric (triaxial) deformation of nuclei. In order to pin down triaxial deformation, it is essential to find the phenomena which are unique in axially-asymmetric shape. In connection with available experimental data on "high- $j$ " configurations in the yrast spectroscopy, some phenomena such as the signature-dependence of  $B(E2: I \rightarrow I-1)$  values in odd- $A$  nuclei and anomalous signature-splitting of Routhians in odd- $A$  and odd-odd nuclei, were theoretically suggested as the evidence for triaxial shape [31]. However, before 2000 a very clear and firm evidence for stable triaxial shape was hardly obtained experimentally.

On the other hand, the two phenomena, wobbling exci-

tation modes and chiral bands, are unique in triaxial shape and were intensively searched for by using the advanced technique developed in high-spin physics. Observation of beautiful wobbling excitation modes was reported in the beginning of the 21st century, while, in my opinion, experimental data which clearly pin down chiral bands have not yet been obtained though several candidates for chiral bands have been reported. In this section I describe the present understanding of these two phenomena.

##### 4.1. Quantized wobbling observed in nuclei

Nuclei with a triaxial shape can rotate about any of the principal axes showing rich spectra of collective rotation. Though the rotation about the axis with the largest moment of inertia is energetically cheapest, while freezing the intrinsic structure a series of rotational bands can be built by transferring some angular momentum to the other two axes. The family of the rotational bands is formulated in terms of vibrational excitations. The classical analog of this wobbling motion is the spinning motion of an asymmetric top, but the motion in the nuclear system is quantized and expressed in terms of the wobbling phonon number ( $n_W$ ). A family of rotational bands with wobbling excitations can be pinned down by specific electromagnetic decay properties between them. This quantized wobbling phonon picture was first proposed by A. Bohr and B. R. Mottelson described in [1].

In 2001 such a wobbling band, a one-phonon wobbling excitation, was discovered in the nucleus  $^{163}\text{Lu}_{92}$  [32]. One year later, in 2002 the next wobbling excitation, a two-phonon rotational band, was reported in the same nucleus [33]. In this experiment high spin states of  $^{163}\text{Lu}$  were populated using a  $^{29}\text{Si}$  beam and a  $^{139}\text{La}$  target. The emitted gamma-rays were measured with the EUROBALL detector system. The electromagnetic nature of the decay transitions from the newly observed band is analyzed and the results clearly show the two-phonon nature of the wobbling motion in good agreement with calculations, in which the intrinsic degree of freedom of the rotational bands in  $^{163}\text{Lu}$  is represented by one highly-aligned quasiproton in the  $i_{13/2}$  shell [34].

The state with high- $j$  aligned particles favors a specific (triaxial) shape [35] depending on the degree of the  $j$ -shell filling. The  $\gamma$ -value favored by the aligned  $i_{13/2}$  proton in  $^{163}\text{Lu}$  is around  $+20^\circ$  (in the so-called "Lund convention" [36]). States with large alignments can easily appear in the neighborhood of the yrast line because of the relatively small rotational angular-momentum (and thereby small rotational energy) needed for building a given total angular-momentum. Furthermore, using a particle-rotor model, in which one quasiparticle of  $i_{13/2}$  protons is coupled to a triaxial core, it was shown [37] that in the presence of one high- $j$  aligned quasiparticle and for the  $\gamma$ -value strongly favored by the fully-aligned high- $j$  particle the wobbling excitation of the collective rotational angular-momentum of the core appears as the yrare band in a certain range of angular momentum and the electromagnetic transitions between the yrast and yrare bands show a unique pattern.

The two-phonon wobbling excitation observed in  $^{163}\text{Lu}$  is one of the most exotic properties of the spinning nu-

cleus. The observation has been possible not least due to an increased efficiency in the detection of gamma-rays with high resolution germanium spectrometers which have been developed and became available during the last decades of the 20th century. The observation of a two-phonon excitation, of which the relevant degree of freedom is collective rotation, amplifies the uniqueness of the finding for nuclear wobbling. The nucleus has revealed its exploitation of the quantal wobbling degree of freedom which proves the existence of triaxial nuclei and adds a new dimension to the description of a rotating nucleus.

Since 2002 the observation of the rotational bands, which showed spectroscopic properties (though often only energies) very similar to those of  $^{163}\text{Lu}$ , were reported in neighboring nuclei including  $^{161,165,167}\text{Lu}$ , indicating the presence of the wobbling bands also in those nuclei. However, the original data on the nucleus  $^{163}\text{Lu}$  are so far most beautiful and best to pin down the characteristic features of not only the energies and spin-parity but also electromagnetic properties and the two-phonon wobbling excitation. Therefore, in the following I briefly describe the observed data on  $^{163}\text{Lu}$  and their interpretation.

The essence of the experimental data on the wobbling excitations of  $^{163}\text{Lu}$  [32, 33, 39] is shown in Figs. 4 and 5, compared with the calculated results obtained by using the particle-rotor model, in which one high-j quasiparticle is coupled to the core of triaxial shape [32, 34, 38]. The moments of inertia and alignments of the three TSD (Triaxial, Strongly Deformed) bands, TSD1, TSD2 and TSD3, are nearly identical, and the intrinsic structure of those TSD bands is understood as containing an aligned high-j ( $= i_{13/2}$ ) proton. TSD2 is identified as the one-phonon ( $n_W = 1$ ) wobbling band built on the yrast TSD1 ( $n_W = 0$ ), while TSD3 as the two-phonon ( $n_W = 2$ ) wobbling band. The identification of the two-phonon band is based on, among others, the unusually large (at this high-spin)  $B(E2; \text{TSD3} \rightarrow \text{TSD2})$  value in agreement with both the phonon picture and the calculated result of the particle-rotor model [34]. It is also noted that very small values of  $B(E2; \text{TSD3}, I \rightarrow \text{TSD1}, I - 2)$  are in agreement with the assignment of TSD3 and TSD1 as  $n_W = 2$  and 0, respectively. The  $\gamma$ -value in the calculation ( $\gamma \approx +20^\circ$ ) was fixed by the observed ratios,  $B(E2; \text{TSD2}, I \rightarrow \text{TSD1}, I - 1)/B(E2; \text{TSD2}, I \rightarrow \text{TSD2}, I - 2)$  and  $B(E2; \text{TSD3}, I \rightarrow \text{TSD2}, I - 1)/B(E2; \text{TSD3}, I \rightarrow \text{TSD3}, I - 2)$ , which are insensitive to used values of moments of inertia but are strongly increasing functions of  $\gamma$ , especially for  $\gamma \geq +20^\circ$ . It should be also mentioned that for nuclei with  $Z \approx 71$  and  $N \approx 94$  "ultimate cranker" calculations [40] predicted triaxial shapes ( $\gamma \approx \pm 20^\circ$ ) with large quadrupole deformations ( $\varepsilon_2 \approx 0.38$ ) for all combinations of parity and signature in the region of angular momenta, which are relevant for the observed TSD bands of  $^{163}\text{Lu}$ . The local minimum with  $\gamma > 0$  is generally lowest, and at the minimum the  $i_{13/2}$  orbital is lowest in energy of the proton system with the favored signature  $\alpha_f = +1/2$  where  $I = \alpha \bmod 2$ .

M1 transitions between  $\Delta n_W = 1$  bands are in general strongly reduced as seen in Fig. 5. This is because in the text-book example [1] namely in the absence of the high-j aligned particle, the total angular-momentum  $\vec{I}$  is the only vector in the system, thus, the magnetic dipole operator

is proportional to  $g\vec{I}$ . Then, M1 transitions should vanish in the case of the isotropic  $g$ -factor in the body-fixed system. In the presence of fully-aligned intrinsic angular-momentum  $\vec{j}$  and when possible quantum-fluctuations are neglected, the argument goes in a similar way to the above case when  $\vec{I}$  above is replaced by  $\vec{R}$  where  $\vec{R}$  expresses the rotational angular-momentum of the even-even core. In contrast, the  $B(E2; n_W, I \rightarrow n_W \pm 1, I - 1)$  value is proportional to  $I^{-1}$ . The observed magnitudes as well as the zigzag pattern of both  $B(M1)$  and  $B(E2)$  values are in good agreement with the wobbling picture obtained from the model consisting of one  $i_{13/2}$  quasiparticle coupled to the triaxial-rotor. In particular, it is interesting to note that in Fig. 5 the zigzag pattern of both  $B(E2)$  and  $B(M1)$  values of  $\Delta I = 1$  transitions in the wobbling regime is opposite to the one in the cranking regime. Furthermore, in the cranking regime one expects that for  $\Delta I = 1$  transitions at high spins the  $B(M1)$  values are the order of unity, while the  $B(E2)$  values are the order of  $I^{-2}$ . Thus, it is seen that the expectation from the cranking model totally disagrees with the observation.

## 4.2. Chiral bands

Spontaneous formation of handedness or chirality is a subject of general interest in molecular physics, the characterization of elementary particles, and in optical physics. The occurrence of chirality in a nuclear structure was considered theoretically [41] and, subsequently, experimental level schemes in some odd-odd nuclei (for example,  $^{134}\text{Pr}_{75}$ ) exhibiting the patterns similar to the predicted ones have been reported [42].

The total Hamiltonian for the nuclear system is taken to be invariant under the exchange of the right- and left-handed geometry. Chirality in triaxial nuclei is characterized by the presence of three angular-momentum vectors, which are generally noncoplanar and thereby make it possible to define chirality. One of the three angular-momenta is the collective rotational angular-momentum, while the other two in odd-odd nuclei are, in practice, angular-momenta of quasiproton and quasineutron in high-j orbits. The hallmark of nuclear chirality is the observation of two almost degenerate  $\Delta I = 1$  rotational bands, chiral bands, having the same parity. Those almost degenerate states are expected to appear only after an appreciable amount of collective rotation develops, while for higher rotational frequency the basis for chirality, namely the noncoplanar structure of the three angular-momenta, will be destroyed. The reason is that in order to make a given large total angular-momentum, it is cheapest to align all constituent angular-momenta to the direction of collective rotation. Thus, chiral bands may be found only in a limited intermediate region of angular-momentum.

Observed so-called chiral bands, two  $\Delta I = 1$  bands, are typically a few hundreds keV apart and one must find a reasonable explanation of this energy difference. Furthermore, though the presence of two close-lying bands may indicate chiral geometry, this geometry can be pinned down in a more definitive way if electromagnetic transition probabilities expected for the chiral bands are experimentally confirmed. The trivial behavior of electromagnetic transition probabilities or the "trivial selection-rule" expected

in general chiral pair-bands is: "For the states with  $I \gg 1$  the corresponding probabilities and moments in the two bands should be identical or in practice almost the same." Namely, when chiral geometry is realized, observed two chiral-degenerate states may be written as

$$|I+\rangle = \frac{1}{\sqrt{2}}(|IL\rangle + |IR\rangle) \quad (3)$$

$$|I-\rangle = \frac{i}{\sqrt{2}}(|IL\rangle - |IR\rangle) \quad (4)$$

where left- and right-handed geometry states are denoted by  $|IL\rangle$  and  $|IR\rangle$ , respectively. For  $I \gg 1$  it is expected that

$$\langle IL|EM|IR\rangle \approx 0 \quad (5)$$

where  $EM$  expresses electromagnetic operators. Then, within the chiral pair-bands one expects

$$B(EM; I_1+ \rightarrow I_2+) \approx B(EM; I_1- \rightarrow I_2-) \quad (6)$$

$$B(EM; I_1+ \rightarrow I_2-) \approx B(EM; I_1- \rightarrow I_2+) \quad (7)$$

In addition, in Ref. [43] the selection rule derived from a special case of odd-odd nuclei, in which the orbits of both odd-neutron and odd-proton are the same high- $j$ , was obtained by using the particle-rotor model in which one-proton- and one-neutron-quasiparticle were coupled to a triaxial core [1]. The majority of observed two close-lying  $\Delta I = 1$  bands in odd-odd nuclei around  $N \approx 75$  [42] belongs to this special case where  $j=h_{11/2}$ . In this case, an additional symmetry exists in the model Hamiltonian and an associated quantum number can be obtained. Using this quantum number a further selection rule for electromagnetic transitions was derived in an unambiguous manner [43]. To my knowledge, two close-lying  $\Delta I = 1$  bands observed in odd-odd nuclei, which approximately satisfy this selection rule, are not yet found.

As a matter of fact, we have not yet observed two close-lying  $\Delta I=1$  bands, of which electromagnetic transition probabilities approximately follow even the "trivial selection-rule". Thus, we have to say that in spite of the nice theoretical idea we have not yet obtained experimental data which show the presence of chiral bands. This fact may come from the transient character of chiral bands, which can survive only in a certain range of angular momentum. The detailed description of our present knowledge about chiral bands together with so far available experimental data will be presented in other contributions to this special issue.

## 5. Nuclear structure as neutron-drip-line approaches

An example of the systematic change of energies of one-particle orbits due to weak binding which we learn in traditional textbooks is Thomas-Ehrman shift. The reduction of the Coulomb energy for the loosely-bound proton orbits and for the unbound resonance states is called Thomas-Ehrman shift. A typical example is: the rather large difference (370 keV) in excitation energies of the  $s_{1/2}$  levels between mirror nuclei,  $E_x = 0.87$  MeV in  $^{17}\text{O}_9$  where the neutron separation energy  $S(n)=4.14$  MeV and  $E_x = 0.50$  MeV in  $^{17}\text{F}_8$  where the proton separation energy  $S(p)=0.60$  MeV, can be explained in terms of the

reduction in Coulomb energy associated with the loosely bound proton [44]. In the case of protons the effect of weak binding on energies and wave functions can be seen only in such very light nuclei because the height of Coulomb barrier becomes increasingly high as  $Z$  increases. In the present section I confine my attention to the neutron-drip-line nuclei despite the significant interest that is also associated with the proton-rich side (among others, nuclear astrophysical importance, neutron-proton correlations in the  $Z \approx N$  region, new opportunities provided by  $p$  and  $2p$  decays).

The study of unstable nuclei, especially neutron-drip-line nuclei which contain very weakly-bound neutrons, has opened a new field in the research of the structure of finite quantum-mechanical systems. The study is important not only because of the interests in nuclear astrophysics such as understanding the production of energy and the synthesis of elements in stars and during stellar events, but also because it provides the opportunity to learn the properties of fermion systems with very loosely bound particles, some density of which can extend to the region far outside the region of the main density of the system. Because the Fermi level of drip-line nuclei lies close to the continuum, both weakly-bound and positive-energy one-particle levels play a crucial role in the many-body correlations of those nuclei.

Among various exciting phenomena which have been explored in the study of the structure of drip-line nuclei I pick up the following two topics in this section. First, we can find the systematic change of neutron shell-structure, as  $S(n)$  decreases and approaches zero or even negative values (namely, one-particle resonances). As a result of it, traditional magic numbers known for stable nuclei may be changed and, furthermore, nuclei with closed-shell configurations in the traditional stable nuclei may become deformed. I describe our understanding of these phenomena in the following first subsection, while in the second subsection I touch the halo phenomena in spherical and deformed nuclei which can be found along the neutron-drip-line having some components of weakly-bound  $\ell=0$  or 1 neutrons.

### 5.1. Shell-structure change and deformation

Recent experimental data obtained by using radioactive ion beams reveal that the neutron numbers such as  $N=8, 20$  and  $28$  are no longer magic numbers in some nuclei toward the neutron-drip-line. In traditional stable nuclei the neutron separation energy  $S(n)$  is typically 7-10 MeV. Thus, the information on one-particle shell-structure around the energy has been easily obtained experimentally. The prominent change of the level structure in the region of  $\varepsilon_j(n) < 7$  MeV can be seen, for example, in Fig. 2-30 of Ref. [44], where the energies of neutron orbits in spherical Woods-Saxon potentials are shown. When the potential strength becomes weaker by decreasing the mass-number  $A$ , thereby decreasing the radius of the potential, eigenvalues of all orbits  $\varepsilon_j(n) < 0$  become less bound. However, neutron-orbits with larger  $\ell$  (thus, larger  $j$ ) lose the binding energy more rapidly than those with smaller ( $j\ell$ ). This is because due to the presence of higher centrifugal barrier the major part of the wave functions of the

orbits with larger ( $j\ell$ ) stays inside the potential and, thus, eigenvalues  $\varepsilon_j(n)$  are more sensitive to the strength of the potential than those of the orbits with smaller ( $j\ell$ ). Taking a finite square-well potential as an example, the probability for bound one-neutron wave-functions to remain inside the potential in the limit of eigenvalues  $\varepsilon_{n\ell}(<0) \rightarrow 0$  is tabulated in Table II.

Since the effective interactions, which can be reliably used in Hartree-Fock (HF) calculations of unstable nuclei far away from the stability line, are not yet established, in the present article we use the Woods-Saxon potential for nuclear one-body potential, of which parameters are taken from p.239 of Ref. [44] unless otherwise stated.

Weakening of the Woods-Saxon potential can be done by reducing either the potential radius or the potential depth. The two ways of weakening change the shape of the potential in respective manners. In Fig. 6 an example of neutron one-particle energies as a function of the depth of a spherical Woods-Saxon potential is given. It is noted that as one-particle energy  $\varepsilon_{\ell j}(<0)$  approaches zero the  $2s_{1/2}$  level approaches the  $1d_{5/2}$  level and may eventually become lower than the latter. Realizing this result the possible neutron magic number  $N=16$  was suggested in Ref. [45].

In the following I use the simple argument: a large one-particle level density around the Fermi level at the spherical point may lead to a deformation. The argument is based on the following known fact: In very light nuclei the many-body pair-correlation may be neglected in a good approximation. Then, nuclei with a few nucleons outside a closed shell can be already deformed, because using the near degeneracy of one-particle levels those nucleons have a possibility of gaining energy by breaking spherical symmetry (Jahn-Teller effect [46]).

Due to the same physics mechanism as the nearly-degenerate  $2s_{1/2}$  and  $1d_{5/2}$  levels in the case of weak binding as shown in Fig. 6, the  $2p_{3/2}$  and  $1f_{7/2}$  levels become nearly degenerate in the case of weak binding or low-lying resonant levels [47, 48]. The Nilsson diagram based on a deformed Woods-Saxon potential which is appropriate for  $^{37}_{12}\text{Mg}_{25}$  [47] is shown in Fig. 7. The  $1f_{5/2}$  and  $2p_{3/2}$  resonant levels for  $\beta=0$  are found at +5.22 and +0.018 MeV with the widths 2.08 and 0.005 MeV, respectively, where one-particle resonance in deformed potentials is defined using the eigenphase formalism [49, 50]. Using the eigenenergy  $\varepsilon(1f_{7/2}) = -0.66$  MeV, the distance between the  $1f_{7/2}$  and  $2p_{3/2}$  levels is 680 keV, which is very small compared with the distance obtained in the case that both levels are well bound, as known from the presence of the magic number  $N=28$  in stable nuclei. This near degeneracy of the  $1f_{7/2}$  and  $2p_{3/2}$  levels at  $\beta=0$  directly means the disappearance of the  $N=28$  energy gap (or magic number) and leads to the fact that the  $N = 20-26$  nuclei with weakly-bound neutrons in the  $1f_{7/2}-2p_{3/2}$  shells may prefer being deformed in the case that the proton configuration allows the deformation [47].

In recent experiments [51] the even-even Mg-isotopes ( $N=22-26$ ) towards the neutron-drip-line are found to be indeed deformed by observing small values of  $E(2_1^+)/E(4_1^+)$  and possible  $E(4_1^+)/E(2_1^+)$  ratios, while the odd- $N$  nuclei,  $^{31}_{10}\text{Ne}_{21}$  and  $^{37}_{12}\text{Mg}_{25}$ , are duly interpreted as deformed p-wave halo nuclei [52, 53].

## 5.2. Spherical and deformed halo phenomena

Interests in nuclear halo phenomena were aroused by the observation of a remarkably large interaction cross section of  $^{11}\text{Li}$ , which suggested a large deformation and/or a long tail in the matter distribution [54]. The long tail is later interpreted as a two-neutron halo phenomenon. The observed neutron-halo structure makes it clear that the extreme difference in the radial motion of weakly-bound  $\ell=0$  and  $\ell=1$  neutrons from the radial distribution of the core particles indicates the approximate decoupling of the halo particles from the core of the nuclear system. The effects of this decoupling on pairing, deformation, and collective rotation is the interesting issue to be studied.

The condition of the formation of neutron halo is that one or two least-bound neutrons have small separation energies, say  $S(n) < 1$  MeV, and some components of low orbital angular-momentum,  $\ell=0$  or 1. If it is one-neutron halo in spherical odd- $N$  nuclei, the wave function of the halo neutron has the  $\ell=0$  or 1 component with the probability close to unity. If it is one-neutron halo in deformed odd- $N$  nuclei, the probability of  $\ell=0$  or 1 component in the halo-neutron wave-function can be considerably smaller than unity. In the latter case the one-neutron wave-function can contain considerable amounts of high- $\ell$  components, which are spatially distributed within the same limited region as the well-bound even-even core nucleus. Thus, in the reactions to which extended tail exclusively contributes, for example Coulomb break-up reactions, one detects only the  $\ell=0$  or 1 component of the one-neutron wave-function. This seems to be the case of Coulomb break-up reactions of  $^{31}_{10}\text{Ne}_{21}$  [52] and  $^{37}_{12}\text{Mg}_{25}$  [53]. Though the deformation of  $^{31}\text{Ne}$  and  $^{37}\text{Mg}$  was predicted in 2007 [47] as a result of the shell-structure of neutron-drip-line nuclei described in the previous subsection, the evidence for deformation of the core nuclei  $^{30}\text{Ne}$  and  $^{36}\text{Mg}$  was recently reported. See Refs. [55] and [51], respectively.

As is seen from the examples of  $^{31}\text{Ne}$  and  $^{37}\text{Mg}$ , if nuclei are deformed, one-neutron halo can be found in many more nuclei with different neutron-numbers  $N$  than in the case that nuclei are limited to be spherical. This is because taking the example of  $\ell=0$  halo, in the spherical case one-particle  $s_{1/2}$ -orbit is obtained only once in every  $N_{ho}=\text{even}$  major-shell, where  $N_{ho}$  expresses the principal quantum-number of the harmonic oscillator (ho). Therefore, spherical  $\ell=0$  halo may be observed only at very special drip-line nuclei, in which a neutron  $s_{1/2}$ -orbit lies around the Fermi level. In contrast, in deformed nuclei all  $\Omega^\pi = 1/2^+$  intrinsic states acquire  $\ell=0$  components induced by the deformation and, thus, all those  $\Omega^\pi = 1/2^+$  orbits have a chance to make a deformed s-wave halo if the orbits are weakly bound [56]. Needless to say, an  $\Omega^\pi = 1/2^+$  orbit can be created from every positive-parity orbits such as  $s_{1/2}$ ,  $d_{3/2}$ ,  $d_{5/2}$ ,  $g_{7/2}$ ,  $g_{9/2}$ , .... Furthermore, the  $\ell=0$  component in a given  $\Omega^\pi = 1/2^+$  orbit increases as the eigenvalue  $\varepsilon_\Omega (<0)$  approaches zero, and the probability of the  $\ell=0$  component approaches unity in the limit of  $\varepsilon_\Omega \rightarrow 0$  [57, 58]. Similar comments apply to the  $\ell=1$  halo, because in the spherical case one-particle  $p_{1/2}$ - and  $p_{3/2}$ -orbits are obtained only once in every  $N_{ho}=\text{odd}$  major shell. In contrast, in deformed nuclei  $\Omega^\pi = 1/2^-$



and  $3/2^-$  intrinsic states originating from every negative-parity orbits such as  $p_{1/2}$ ,  $p_{3/2}$ ,  $f_{5/2}$ ,  $f_{7/2}$ ,  $h_{9/2}$ ,  $h_{11/2}$ , ..... acquire  $\ell=1$  components induced by the deformation, and all these orbits may make deformed  $\ell=1$  halo if the orbits are weakly bound. The  $\ell=1$  component in given  $\Omega^\pi = 1/2^-$  and  $3/2^-$  orbits increases also in the limit of  $\varepsilon_\Omega(<0) \rightarrow 0$ , but the amount of increase depends on both one-particle orbits and potentials.

## 6. Oblate ground state of even-even nuclei

It is known that almost all known deformed even-even nuclei in the medium-heavy mass region can be interpreted in terms of prolate axially-symmetric dominantly quadrupole deformed shape. In the absence of pair correlation one obtains the number of prolate systems approximately equal to that of oblate ones in the simple models such as one-major-shell harmonic-oscillator or single-j shell. However, when HF calculations with appropriate effective interactions are performed in many well-bound nuclei, the dominance of prolate shape except for very light nuclei is obtained in agreement with the experimental observations. In my opinion, the nature of the element responsible for the overwhelming dominance of prolate shape has not yet been adequately understood.

Figure 6-48 of Ref. [1] expresses the single-particle spectrum for axially-symmetric quadrupole-deformed oscillator potentials and the resulting magic numbers for  $(\omega_\perp : \omega_3) = (1:2)$ ,  $(1:1)$  and  $(2:1)$ . The magic numbers for spherical shape  $(1:1)$  are well known in textbooks for years. On the other hand, the prominent shell-structure with the prolate shape  $(2:1)$  has played an important role in understanding the occurrence of both fission isomers [27, 1] and high-spin superdeformed bands. These phenomena have provided striking evidence for the shell structure in nuclear potentials with much larger deformations than those encountered in the ground states of heavy nuclei. Though neither spin-orbit potential nor surface effects, which are important elements in nuclear potentials, are present, the shell structure seen in the oscillator potential has helped us to understand the physics in a simple terminology. In the present section it is shown that the possible oblate shape of the ground states of light well-bound nuclei, say  $Z < 30$ , can also be easily understood in terms of the "Nilsson diagram" based on the deformed oscillator potential.

Recently, the neutron-rich nucleus  $^{42}_{14}\text{Si}_{28}$  was reported to show a rotational spectrum [59], namely the ratio of observed excitation energies is  $E(4_1^+)/E(2_1^+) = 2.93(5)$  where  $E(I_1^\pi)$  expresses the excitation energy of the lowest level with the spin-parity  $I^\pi$ , though the spin-assignment of the  $4^+$  state is not yet actually pinned down experimentally. The observed value of  $E(2_1^+)$ , 770 keV, is not small compared with possibly prolate Mg isotopes ( $^{34,36,38}\text{Mg}$ ), of which  $E(2_1^+)$  is around 650 keV. The relatively low moment of inertia corresponding to  $E(2_1^+) = 770$  keV may indicate an oblate deformation. One may wonder the reason why the nucleus with the neutron-number  $N=28$  is deformed and not spherical, as the neutron-number 28 is a well-known magic-number in the j-j coupling shell-model and the observed neutron separation energy of  $^{42}\text{Si}$ ,  $S(n) = 3.6$  MeV, is not small.

When even-even nuclei in the range of  $6 \leq Z \leq 30$ , of which the observed electric quadrupole moment of the first-excited  $2^+$  state is clearly positive corresponding to an oblate shape (or a fluctuation towards oblate shape), are looked for, one finds only five nuclei:  $^{12}_6\text{C}_6$ ,  $^{28}_{14}\text{Si}_{14}$ ,  $^{34}_{16}\text{S}_{18}$ ,  $^{36}_{18}\text{S}_{18}$  and  $^{64}_{28}\text{Ni}_{36}$ . The proton and neutron numbers of these five nuclei remind us of the magic numbers of oblate deformation with the frequency ratio  $(\omega_\perp : \omega_3) = (1:2)$  and  $(2:3)$  in the deformed oscillator potential. See Figure 6-48 of [1]. Namely, the magic numbers are  $Z = N = 6, 14, 26, 44, \dots$  for the  $(1:2)$  deformation while  $N = Z = 6, 8, 14, 18, 28, 34, 48, \dots$  for the  $(2:3)$  deformation. When the neutron and/or proton numbers are equal to one of those magic numbers, the system in the deformed potential is supposed to be especially stable for respective  $(\omega_\perp : \omega_3)$  deformations, though the total deformation is determined by both proton and neutron numbers. The deformation parameter  $\beta$  of the ground state obtained from experimental data is relatively large for lighter nuclei, but certainly smaller than  $|\beta| = 0.7$ . The deformation parameter  $\delta_{osc} = (\omega_\perp - \omega_3)/\bar{\omega}$ , where  $\bar{\omega} = (2\omega_\perp + \omega_3)/3$ , is equal to  $-0.43$  and  $-0.75$  for the ratio  $(\omega_\perp : \omega_3) = (1:2)$  and  $(2:3)$ , respectively. Thus, except for extremely light nuclei the magic numbers for the  $(2:3)$  shape may be more realistic than those for the  $(1:2)$  shape, considering  $\delta_{osc} \approx \beta$ .

In Fig. 8 the calculated Nilsson diagram for  $^{42}_{14}\text{Si}_{28}$ , which is obtained based on realistic Woods-Saxon potentials, is shown [60]. From Fig. 8 it is seen that the energy difference,  $\varepsilon(2p_{3/2}) - \varepsilon(1f_{7/2})$ , is only 1.65 MeV, which is smaller than the standard  $N=28$  energy gap known in the j-j coupling shell model. Indeed, the energy gap on the oblate side, which is largest around  $\beta = -0.4$ , is appreciably larger than the gap at  $\beta = 0$ . Large energy gaps on the oblate side around  $\beta = -0.4$  occur at  $N = 14, 18$  and  $28$ . Those neutron-numbers are in fact exactly the magic numbers for the  $(2:3)$  deformation of the deformed oscillator potential, though the Woods-Saxon potentials used for drawing Fig. 8 of course contain the spin-orbit potential with the standard strength. In contrast, it should be noted that the neutron numbers, at which large energy gaps are found on the prolate side of Fig. 8, such as  $N = 12, 16, 24$  and  $28$  around  $\beta = +0.4$  have no relation with the magic numbers for the prolate  $(\omega_\perp : \omega_3) = (3:2)$  deformation of the oscillator potential,  $N = \dots, 14, 22, 26, 34, \dots$ . See also Fig. 9 for the particle numbers in slightly heavier nuclei, at which large energy gaps are found in Nilsson diagrams based on realistic potentials, in comparison with those based on the oscillator potential.

For  $N=28$  on the oblate side of Fig. 8 four doubly-degenerate Nilsson levels with  $N_{ho}=3$  are occupied, while none of  $N_{ho}=2$  orbits are unoccupied. This is the same configuration as the one at the magic number 28 of the  $(2:3)$  deformation of the oscillator potential. In short, the possible oblate deformation of  $^{42}\text{Si}$  can be understood as a result of the combination of the facts: (i) Narrowing the spherical  $N=28$  magic number due to the shell-structure change in very neutron-rich nuclei; (ii)  $N=28$  remains as "a magic number" for the moderate-size ( $\beta \approx -0.4$ ) oblate deformation in realistic nuclear potentials, and it is in fact the magic number for the oblate  $(2:3)$  deformation of the oscillator potential; (iii) Oblate shape is much favored also

by the proton number  $Z=14$ . Note that the shell structure for protons in lighter well-bound nuclei is not so different from that for well-bound neutrons.

The different correspondence between the realistic Woods-Saxon potential and the oscillator potential for the prolate deformation from for the oblate deformation seems to come mainly from the different behavior of the Nilsson one-particle levels connected to the high- $j$  shell (the  $1f_{7/2}$  shell in the present case) on the prolate side from on the oblate side. The different behavior of the high- $j$  Nilsson levels was discussed in detail in [61] in relation to the numbers of oblate/prolate nuclei. Due to the sign of nuclear spin-orbit potential a given high- $j$  orbit in a spherical potential is strongly pushed down relative to other orbits belonging to the same oscillator major shell. Consequently, on the oblate side the unique shell-structure coming from the presence of the high- $j$  orbit in realistic potentials is disturbed soon after deformation sets in, and large energy gaps in the Nilsson diagram occur at the particle numbers similar to those in the oscillator potential. In contrast, on the prolate side the shell structure originating from the high- $j$  orbit in realistic potentials survives in the range of the realistic quadrupole deformation and, thus, the particle number, at which a large energy gap occurs, is considerably different from that of the oscillator potential.

Because of the simple property of the shell structure on the oblate side mentioned above, which is common to the Woods-Saxon potentials with realistic parameters (and also realistic HF potentials), one may pretty reliably predict the light nuclei, of which the ground state may have an oblate shape. A good candidate for the oblate shape of light nuclei, which is immediately obtained from the above discussion, is  ${}^{20}_6\text{C}_{14}$ .

## 7. Conclusions and discussions

In my understanding the interplay between one-particle and collective degrees of freedom has been a fundamental theme in the nuclear-structure physics of Bohr and Mottelson. In all topics described in the present article the interplay is explicitly recognized. Taking an example of particle-vibration coupling presented in Sec. II, first of all the coupling gives the relation between the vibration of an even-even nucleus and that of the neighboring odd- $A$  nuclei. At the same time the coupling specifies the structure of the vibration of the even-even nucleus itself such as the transition density, which in turn gives the octupole vibrational strength. The self-consistent description of the vibration in terms of one-particle motion has to be satisfied. In the case that the coupling is weak enough to be treated by perturbation, it is easy to quantitatively check the validity of our understanding of the vibration.

The unique role played by particles in high- $j$  orbits is noticeable in almost all topics. Some unique features of particles in high- $j$  orbits are: approximately high- $j$  wavefunctions not only for the practical size of quadrupole deformation but also under an appreciable amount of rotation; large Coriolis coupling; strong alignment immediately after rotation sets in; unique contribution to octupole vibrations; in case of full alignment of one high- $j$  quasiparticle a given  $\gamma$  deformation is preferred as a function of shell-filling; unique contributions to the shell-

structure for prolate shape and for oblate shape, respectively; and so on.

Though the idea of particle-vibration coupling itself can be applied to any kind of vibrations in nuclei, numerical applications have been so far done extensively in the isoscalar shape oscillations. When the vibration is the isoscalar quadrupole oscillation in spherical nuclei, the associated particle-vibration coupling is often so strong that it cannot be treated by perturbation. In the present article the particle-vibration coupling, in which the vibration is a typical isoscalar octupole shape-oscillation, the lowest excited  $3^-$  state of  ${}^{208}_{82}\text{Pb}_{126}$ , is chosen. In this case most data can be analyzed by the perturbation treatment of the coupling. Thanks to the richness of available experimental data on the octupole-vibrations in neighboring nuclei of  ${}^{208}\text{Pb}$ , I believe we have confirmed that Bohr and Mottelson's basic idea of the shape oscillations and the associated particle-vibration coupling in nuclei is definitely on the right track.

Nuclear high-spin physics, in particular the yrast spectroscopy, was very actively and successfully developed during the last three decades of the 20th century, together with the tremendous progress in multi-gamma-ray detectors,  $4\pi$  or  $8\pi$  spectrometers and heavy-ion accelerators. At the beginning people were just fascinated by studying various kinds of rotational bands obtained from the analysis of observed discrete  $\gamma$ -rays. The analysis of the data around the deformed ground-state was carried out based on Nilsson diagrams, while at higher spins it was often done based on Routhian diagrams. A clear evidence for Mottelson-Valatin effect [62], which was wondered once to be the origin of back-bending phenomena, was of course looked for. However, a clear-cut evidence for the phase transition might have been difficult to be seen in finite systems such as nuclei. After the discovery of the superdeformed (2:1) band in 1986, hyperdeformed (3:1) bands were looked for, but the analysis of further complicated discrete and continuum  $\gamma$ -rays has been so far unsuccessful in drawing any clear conclusion.

Experimental findings of quantized wobbling modes are the result of the technology developed in high-spin physics. The wobbling mode in  ${}^{163}\text{Lu}$  is the first one observed in nuclei, and it is even now the most beautiful and complete one. The presence of one aligned  $i_{13/2}$  proton in the intrinsic configuration of  ${}^{163}\text{Lu}$  certainly helped the mode to appear around the yrast line so as to be found more easily.

The electromagnetic properties of observed two close-lying  $\Delta I = 1$  rotational bands are being explored presently by several experimental groups. So far, whenever the electromagnetic transition probabilities were measured, they did not follow even the "trivial selection-rule". However, if the close-lying  $\Delta I = 1$  bands are not interpreted as chiral pair-bands, one may wonder what they are.

Drip-line physics with halo phenomena is relatively newly-developed area in the study of nuclear structure, as a result of radioactive ion beam facilities constructed all over the world. It has given us the opportunity to learn the properties of fermion systems with very loosely bound particles. The heaviest odd- $N$  halo nucleus so far known is  ${}^{37}\text{Mg}$ , which is interpreted as the deformed p-wave halo. In heavier nuclei the ratio of the fraction of

the particles, which lie in the extended region far outside the region of the main density of the system, to the total number of particles becomes smaller. Nevertheless, the reactions such as Coulomb break-up, which are extremely sensitive to the density far outside the region of the main density, may still easily detect the halo structure. Then, besides the possible halo related to the  $2p_{1/2}$  level, the interesting region of possible one-neutron halo heavier than  $^{37}\text{Mg}$  will be the neutron-drip-line nucleus with  $N \approx 50$  coming from the weakly-bound  $3s_{1/2}$  orbit if the shape is limited to be spherical. In contrast, if we look for the prolately deformed region as a result of near-degeneracy of the  $1g_{9/2}$ ,  $3s_{1/2}$  and  $2d_{5/2}$  orbits in the spherical limit, a deformed  $s$ -wave halo may be expected for the lowest-lying  $\Omega^\pi = 1/2^+$  orbit of the  $N_{ho}=4$  major shell, which will lie around the Fermi level of neutron-drip-line nuclei with  $N \approx 40$ . See Fig. 9.

The reason for the overwhelming dominance of prolate shape compared with oblate shape except for very light nuclei has not really pinned down. The clear difference of the splitting of one-particle levels coming from high- $j$  orbits on the prolate side from on the oblate side may have something to do with the dominance. Due to the unique shell-structure on the oblate side the particle numbers, at which the large energy gap occurs on the oblate side of the Nilsson diagram of realistic potentials, can be reliably guessed from the magic numbers of the deformed oscillator potential. In this connection, it would be interesting to know whether the shape of  $^{20}_6\text{C}_{14}$  is oblate or not.

At the end, once more I would like to express my sincere and heartfelt thanks to Aage Bohr and Ben Mottelson for guiding me for years to study and enjoy physics.

## References

- [1] A. Bohr and B. R. Mottelson, *Nuclear Structure* (Benjamin, Reading, MA, 1975), Vol. II.
- [2] I. Hamamoto, *Physics Reports* **10C**, no.2, (1974).
- [3] A. R. Barnett and W. R. Phillips, *Phys. Rev.* **186**, 1205 (1969).
- [4] O. Hausser, F. C. Khanna and D. Ward, *Nucl. Phys.* **A194**, 113 (1972).
- [5] E. Grosse *et al.*, *Nucl. Phys.* **A174**, 525, (1971).
- [6] J. W. Hertel, D. G. Fleming, J. P. Schiffer and H. E. Gove, *Phys. Rev. Lett.* **23**, 488 (1969).
- [7] I. Hamamoto, *Phys. Lett.* **66B**, 410, (1977).
- [8] M. Nagao, in: *Proc. of the Intern. Conf. on Nuclear Structure Studies using Electron Scattering and Photoreaction*, eds. K. Shoda and H. Ui (Sendai, 1972) p.121.
- [9] J. H. Heisenberg and I. Sick, *Phys. Lett.* **32B**, 249 (1970).
- [10] M. Piiparinen *et al.*, *Z. Phys.* **A309**, 87, (1982).
- [11] P. Kleinheinz, *et al.*, *Phys. Rev. Lett.* **48**, 1457, (1982).
- [12] S. G. Nilsson, *Mat. Fys. Medd. Dan. Vid. Selsk.* **29**, no.16, (1955).
- [13] S. A. Moszkowski, *Phys. Rev.* **99**, 803, (1955).
- [14] K. Gottfried, *Phys. Rev.* **103**, 1017, (1956).
- [15] A. Johnson, H. Ryde and J. Sztarkier, *Phys. Lett.* **B34**, 605, (1971); A. Johnson, H. Ryde and S. A. Hjorth, *Nucl. Phys.* **A179**, 753 (1972).
- [16] S. Cohen, F. Plasil and W. J. Swiatecki, *Ann. Phys.* **82**, 557 (1974).
- [17] A. Bohr, Nobel Lecture, Dec.11, 1975 (Nobelstiftelsen 1976).
- [18] A. Bohr and B. R. Mottelson, *Phys. Today*, **32**, 25 (1979).
- [19] I. Hamamoto, *Treatise on Heavy-Ion Science*, Vol.3, 313, (Plenum Publishing Corporation, 1985).
- [20] J. D. Garrett, G. B. Hagemann and B. Herskind, *Ann. Rev. Nucl. Part. Sci.* **36**, 419 (1986).
- [21] A. Bohr and B. R. Mottelson, *Phys. Scri.* **10A**, 13 (1974).
- [22] R. Bengtsson, I. Hamamoto and B. R. Mottelson, *Phys. Lett.* **73B**, 259 (1978).
- [23] R. Bengtsson and S. Frauendorf, *Nucl. Phys.* **A327**, 139 (1979).
- [24] I. Hamamoto, *NUCLEAR STRUCTURE 1985*, p.129, *Proc. of the Niels Bohr Centennial Conference*, Copenhagen, May, 1985 (NORTH-HOLLAND).
- [25] I. Hamamoto, *Nucl. Phys.* **A271**, 15, (1976).
- [26] P. Twin *et al.*, *Phys. Rev. Lett.* **57**, 811 (1986).
- [27] S. M. Polikanov *et al.*, *J. Exptl. Theoret. Phys. (USSR)* **42**, 1464 (1962); *Transl. Soviet Phys. JETP* **15**, 1016 (1962).
- [28] P. J. Nolan and P. J. Twin, *Ann. Rev. Nucl. Part. Sci.* **38**, 533 (1988).
- [29] R. V. F. Janssens and T. L. Khoo, *Ann. Rev. Nucl. Part. Sci.* **41**, 321 (1991).
- [30] Some experimental data are collected in: K. Heyde and J. L. Wood, *Rev. Mod. Phys.* **83**, 1467 (2011).
- [31] For example, see: I. Hamamoto, *Nucl. Phys.* **A520**, 297c (1990).
- [32] S.W. Ødegård *et al.*, *Phys. Rev. Lett.* **86**, 5866 (2001).

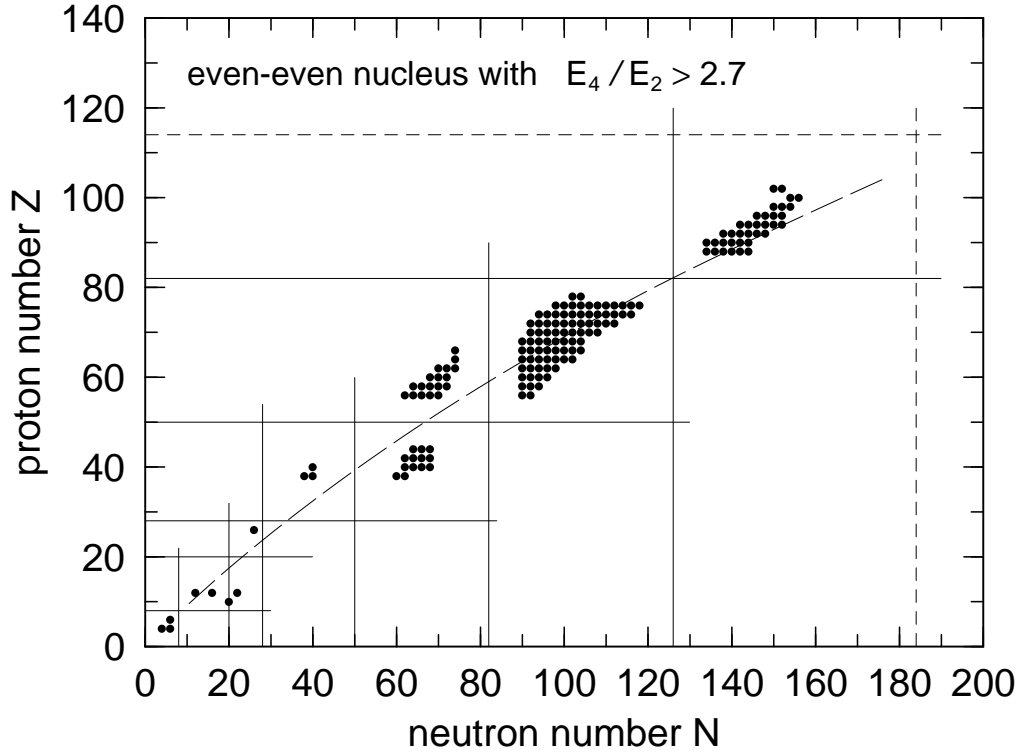
- [33] D. R. Jensen *et al.*, Phys. Rev. Lett. **89**, 142503 (2002).
- [34] I. Hamamoto, Phys. Rev. C **65**, 044305 (2002).
- [35] I. Hamamoto and B. R. Mottelson, Phys. Lett. **B127**, 281 (1983).
- [36] G. Andersson *et al.*, Nucl. Phys. **A268**, 205 (1976).
- [37] I. Hamamoto, Phys. Lett. **B193**, 399 (1987).
- [38] D. R. Jensen *et al.*, Nucl. Phys. **A703**, 3 (2002).
- [39] G. B. Hagemann, private communications.
- [40] H. Schnack-Petersen *et al.*, Nucl. Phys. **A594**, 175 (1995).
- [41] S. Frauendorf and J. Meng, Nucl. Phys. **A617**, 131 (1997).
- [42] K. Starosta *et al.*, Phys. Rev. Lett. **86**, 971 (2001).
- [43] T. Koike, K. Starosta and I. Hamamoto, Phys. Rev. Lett. **93**, 172502 (2004).
- [44] A. Bohr and B. R. Mottelson, *Nuclear Structure* (Benjamin, Reading, MA, 1969), Vol. I.
- [45] A. Ozawa, T. Kobayashi, T. Suzuki, K. Yoshida, and I. Tanihata, Phys. Rev. Lett. **84**, 5493 (2000).
- [46] H. Jahn and E. Teller, Proc. R. Soc. London, Ser. **A161**, 220 (1937).
- [47] I. Hamamoto, Phys. Rev. **C76**, 054319 (2007).
- [48] I. Hamamoto, Phys. Rev. **C85**, 064329 (2012).
- [49] R. G. Newton, *Scattering Theory of Waves and Particles* (McGraw-Hill, New York, 1966).
- [50] I. Hamamoto, Phys. Rev. **C72**, 024301 (2005); **C73**, 064308 (2006).
- [51] P. Doornenbal *et al.*, Phys. Rev. Lett. **111**, 212502 (2013).
- [52] T. Nakamura *et al.*, Phys. Rev. Lett. **103**, 262501 (2009); **112**, 142501 (2014).
- [53] N. Kobayashi *et al.*, Phys. Rev. Lett. **112**, 242501 (2014).
- [54] I. Tanihata *et al.*, Phys. Rev. Lett. **55**, 2676 (1985).
- [55] P. Fallon *et al.*, Phys. Rev. **C81**, 041302 (2010).
- [56] I. Hamamoto and B. R. Mottelson, C. R. Physique **4**, 433 (2003).
- [57] T. Misu, W. Nazarewicz and S. Åberg, Nucl. Phys. **A614**, 44 (1997).
- [58] I. Hamamoto, Phys. Rev. **C69**, 041306(R) (2004).
- [59] S. Takeuchi *et al.*, Phys. Rev. Lett. **109**, 182501 (2012).
- [60] I. Hamamoto, Phys. Rev. **C89**, 057301 (2014).
- [61] I. Hamamoto and B. R. Mottelson, Phys. Rev. **C79**, 034317 (2009).
- [62] B. R. Mottelson and J. G. Valatin, Phys. Rev. Lett. **5**, 511 (1960).

Table 1: The decay scheme of the septuplet  $(h_{9/2} 3^-) I^\pi$  in  $^{209}\text{Bi}$ . In the second column the calculated and experimental energy shifts from the unperturbed energy 2.614 MeV are shown. In the third, fourth and fifth columns the values of  $B(E\nu)$  and  $B(M\nu)$  are shown in respective Weisskopf units, where the number without brackets is the calculated value and the one with brackets is the experimental value taken from Ref. [6]. The numbers in parentheses express the branching ratios. In the calculation the values  $[e_{eff}^p(E1)]^2 = 0.14 e^2$ ,  $g(3^-) = 0.58$ ,  $g_{s,eff}(M\nu) = 0.35$   $g_{s,free}$  and  $e_{eff}^p(E3) = 1.3 e$  were used. The calculated results are taken from Ref. [2].

$I^\pi$	$\delta E_{calc}/\delta E_{exp}$ (keV)	$\rightarrow 9/2^- (g.s.)$	$\rightarrow 7/2^- (0.89 \text{ MeV})$	$\rightarrow 13/2^+ (1.60 \text{ MeV})$
$3/2^+$	-190/-120	20.8 E3 (99) [(100)]	$3.8 \times 10^{-2}$ M2 (1)	
$9/2^+$	-89/-49	$1.1 \times 10^{-3}$ E1 (99) [(1.4±1.8) $\times 10^{-3}$ E1 (100)]	$3.1 \times 10^{-5}$ E1 (1) [ $\leq (2.5\pm 3) \times 10^{-4}$ E1 ( $\leq 5$ )]	
$7/2^+$	-6/-29	$1.5 \times 10^{-5}$ E1 (30) [(1.4±0.8) $\times 10^{-5}$ E1 (33)]	$1.2 \times 10^{-4}$ E1 (70) [(1±0.5) $\times 10^{-4}$ E1 (67)]	
$11/2^+$	-31/-14	$6.1 \times 10^{-4}$ E1 (99.5) [(1.7±1) $\times 10^{-4}$ E1 (85)]		$3.6 \times 10^{-3}$ M1 (0.5) [(6.2±4) $\times 10^{-2}$ M1 (15)]
$13/2^+$	-63/-14	30.2 E3 + $3.5 \times 10^{-3}$ M2 (14) [(1)]		$6.7 \times 10^{-3}$ M1 (86) [(1.1±0.6) $\times 10^{-1}$ M1 (99)]
$5/2^+$	+7/+4	31.9 E3 + $8.6 \times 10^{-3}$ M2 (49) [(41)]	$2.2 \times 10^{-6}$ E1 (51) [(2.2±1) $\times 10^{-6}$ E1 (59)]	
$15/2^+$	+156/+130	30.3 E3 (55) [(53)]		$9.3 \times 10^{-4}$ M1 (45) [(7±2) $\times 10^{-4}$ M1 (47)]

Table 2: Probability for bound one-neutron wave-functions to remain inside a finite square-well potential with radius  $R_0$ , in the limit that eigenenergies  $\varepsilon_{n\ell}$  ( $< 0$ ) approaches zero.

$\ell$	0	1	2	3	$\ell (\neq 0)$
$\int_0^{R_0}  R_{n\ell}(r) ^2 dr$	0	1/3	3/5	5/7	$(2\ell - 1)/(2\ell + 1)$



*Fig. 3:* Regions of deformed even-even nuclei. Even-even nuclei have the ground-state spin-parity  $0^+$ , without exception. The overwhelming majority of these has  $2^+$  first excited state. Writing the excitation energies of the lowest-lying  $2^+$  and  $4^+$  states as  $E(2_1^+)$  and  $E(4_1^+)$ , the filled circle denotes even-even nuclei, in which  $E(4_1^+)/E(2_1^+) > 2.7$ . The data are taken from <http://www.nndc.bnl.gov/ensdf/>. The line of  $\beta$ -stability is indicated by the thin long-dashed curve. The thin straight lines parallel to the x and y axes show the magic numbers of protons and neutrons, which are known in nuclei along the  $\beta$ -stability line. Except for very light nuclei ( $Z \leq 8$ ) the neutron drip line, at which nuclei become unstable for neutron emission, is not known experimentally. The border of deformed nuclei plotted for the neutron-rich region of medium-heavy nuclei is often equal to the border of neutron-rich nuclei, for which the energy of the  $4_1^+$  state is presently known.

# Wobbling excitations in $^{163}\text{Lu}$

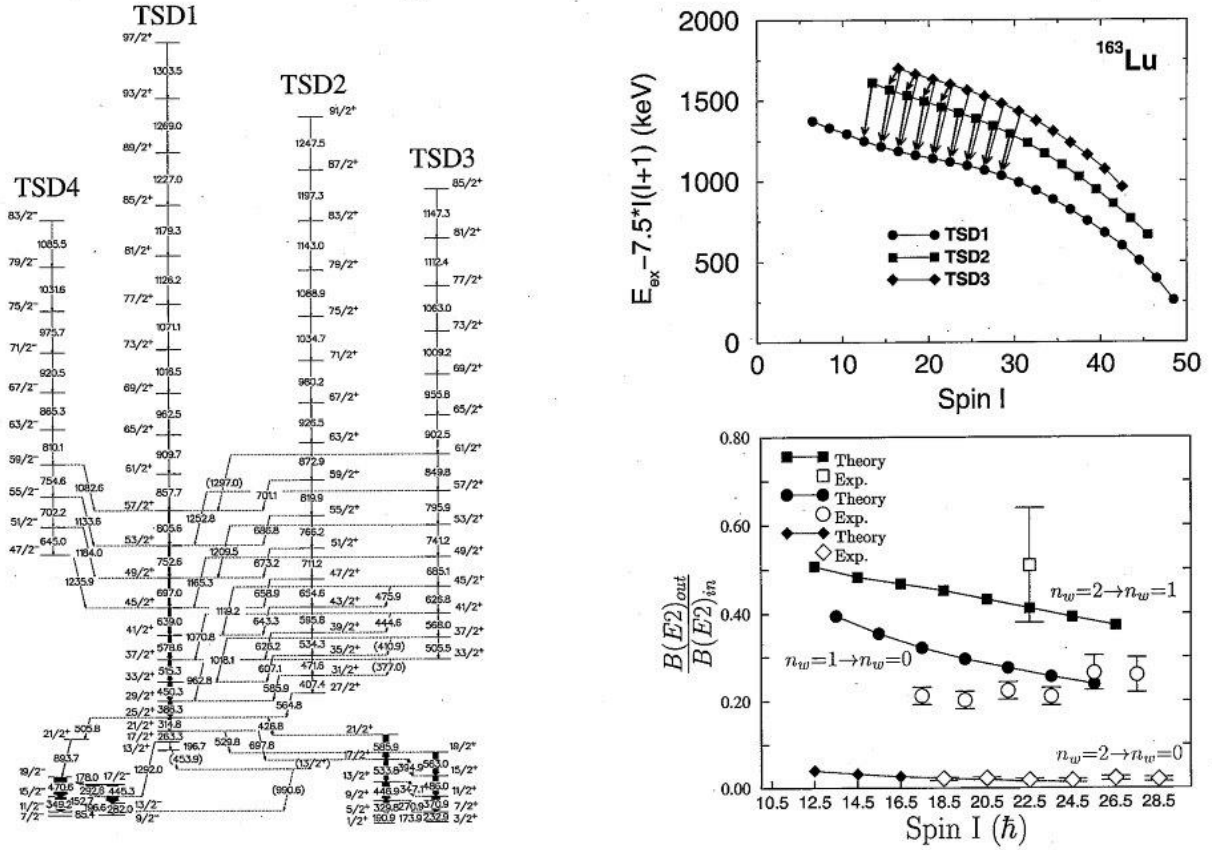


Fig. 4: Experimental data on the wobbling excitations in  $^{163}\text{Lu}$ . The figures on the left and the upper right are made from measured level scheme, while measured  $B(E2)$  values in comparison with calculated  $B(E2)$  values are shown in the figure on the lower right.  $B(E2)_{\text{in}}$  expresses  $B(E2; n_W, I \rightarrow n_W, I-2)$ , while  $B(E2)_{\text{out}}$  denotes  $B(E2; n_W, I \rightarrow n_W - 1, I-1)$  or  $B(E2; n_W, I \rightarrow n_W - 2, I-2)$ . TSD2 is identified as the one-phonon ( $n_W=1$ ) wobbling band built on the yrast TSD1 ( $n_W=0$ ), while TSD3 as the two-phonon ( $n_W=2$ ) wobbling band. The author expresses her thanks to G. B. Hagemann for the present figure.

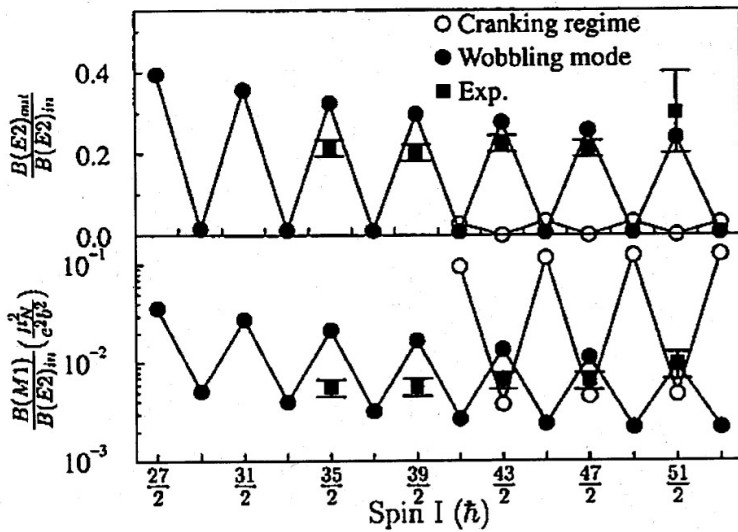
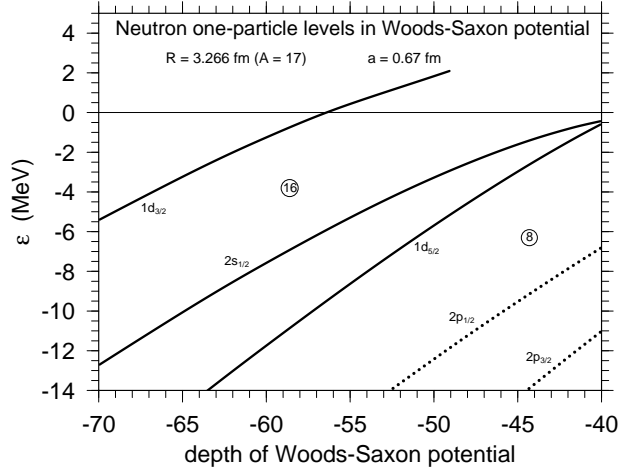
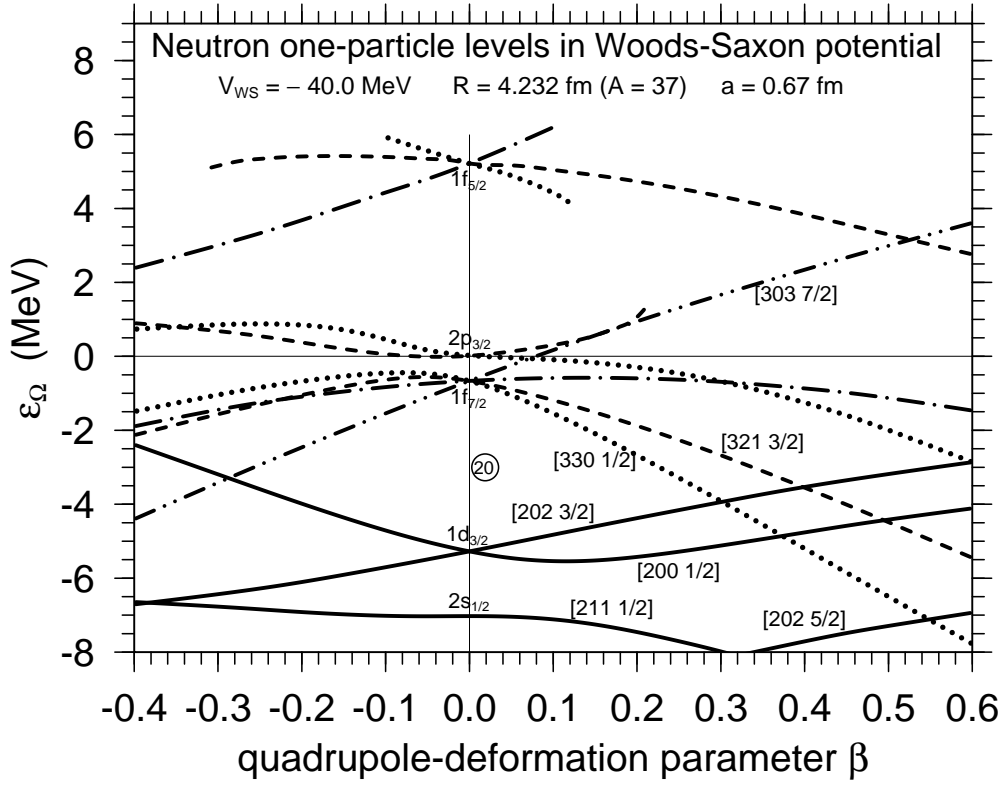


Fig. 5: Experimental electromagnetic properties of the transitions connecting TSD2 with TSD1 are shown by filled squares with experimental errors.  $B(E2)_{\text{out}}$  represents  $B(E2; \text{TSD2}, I \rightarrow \text{TSD1}, I-1)$ , and  $B(M1)$  expresses  $B(M1; \text{TSD2}, I \rightarrow \text{TSD1}, I-1)$ , while  $B(E2)_{\text{in}}$  denotes  $B(E2; \text{TSD2}, I \rightarrow \text{TSD2}, I-2)$ . Filled circles denote calculated values obtained from the particle-rotor model, of which the result shows that the wobbling excitation becomes the lowest unfavored-signature ( $\alpha_u$ ) state in the relevant angular-momentum region, while open circles represent calculated values obtained by using cranking model. The figure is taken from Ref. [32]



*Fig. 6:* Calculated neutron one-particle energies as a function of the depth of spherical Woods-Saxon potentials. The  $\ell=2$  one-particle resonant level continues to be well defined up to  $\varepsilon = 2$  MeV, while there is no one-particle resonance for  $\ell=0$ . The parameters of the Woods-Saxon potential except for the depth are kept constant and are designed approximately for the nucleus  $^{17}\text{C}$ , for which the realistic depth should be around  $-40$  MeV. The figure is taken from Ref. [47].





*Fig. 7:* Calculated neutron one-particle levels as a function of axially-symmetric quadrupole deformation. Parameters of the Woods-Saxon potential are designed approximately for the nucleus  $^{37}\text{Mg}$ . Note that the  $2p_{3/2}$  level at  $\beta=0$  is a one-particle resonant level with the energy  $+0.018$  MeV. The  $2p_{1/2}$  resonant level is not obtained at  $\beta=0$ , and for  $\beta \neq 0$  no  $\Omega^\pi = 1/2^-$  one-particle level connected to the possible  $2p_{1/2}$  level can survive as a resonant level. The  $\Omega^\pi = 1/2^-$  levels are denoted by dotted curves, the  $\Omega^\pi = 3/2^-$  levels by dashed curves, the  $\Omega^\pi = 5/2^-$  levels by dot-dashed curves, and the  $\Omega^\pi = 7/2^-$  levels by dot-dot-dashed curves, while positive-parity levels are plotted by solid curves. The  $\Omega^\pi = 1/2^-$  resonant level connected to the one-particle resonant  $1f_{5/2}$  level at  $\beta=0$  cannot survive as a resonance for  $\beta > 0.12$  because of the increasing  $\ell=1$  component inside the nuclear radius. The definition of one-particle resonance in a deformed potential can be found in [49, 50]. The figure is taken from Ref. [47].

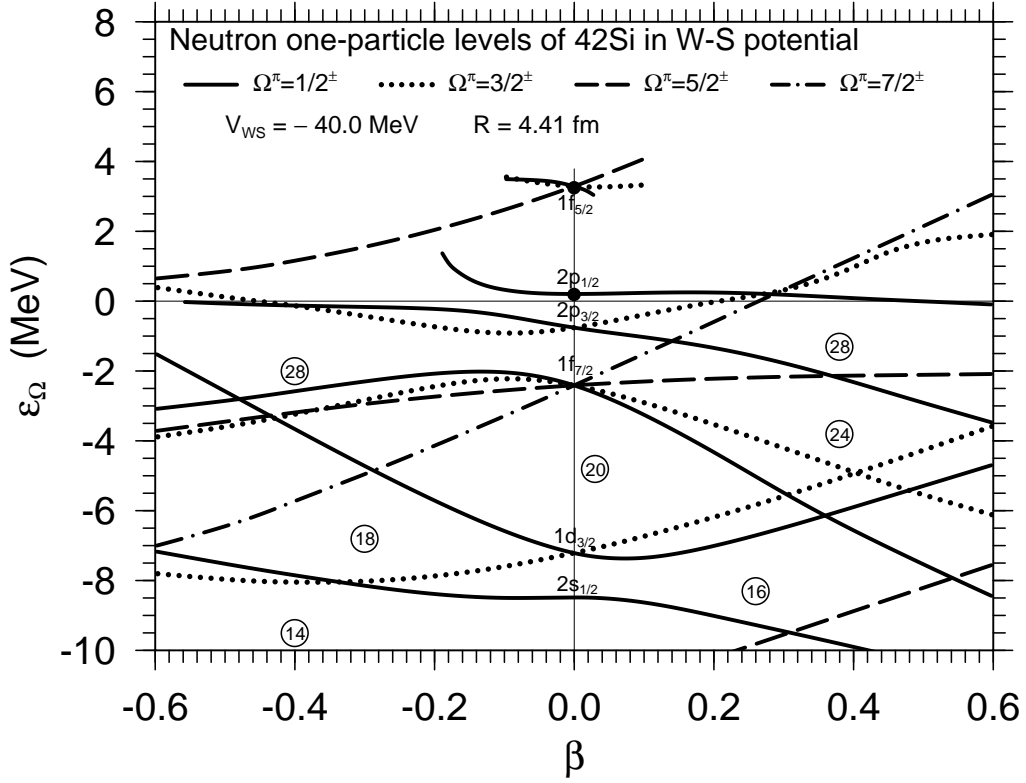


Fig. 8: Calculated one-particle energies for neutrons of  $^{42}_{14}\text{Si}_{28}$  as a function of axially-symmetric quadrupole deformation. Bound one-particle energies at  $\beta=0$  are  $-8.50$ ,  $-7.24$ ,  $-2.42$  and  $-0.77$  MeV for the  $2s_{1/2}$ ,  $1d_{3/2}$ ,  $1f_{7/2}$  and  $2p_{3/2}$  levels, respectively, while one-particle resonant  $2p_{1/2}$  and  $1f_{5/2}$  levels are obtained at  $+0.20$  MeV with the width of  $0.20$  MeV and  $+3.25$  MeV with the width of  $0.58$  MeV, respectively, which are denoted by filled circles. One-particle resonant energies for  $\beta \neq 0$  are not plotted unless they are important for the present discussion. For simplicity, calculated widths of one-particle resonant levels are not shown. The neutron numbers, which are obtained by filling all lower-lying levels, are indicated with circles. The parity of levels can be seen from the  $\ell$  values denoted at  $\beta=0$ ;  $\pi = (-1)^\ell$ .

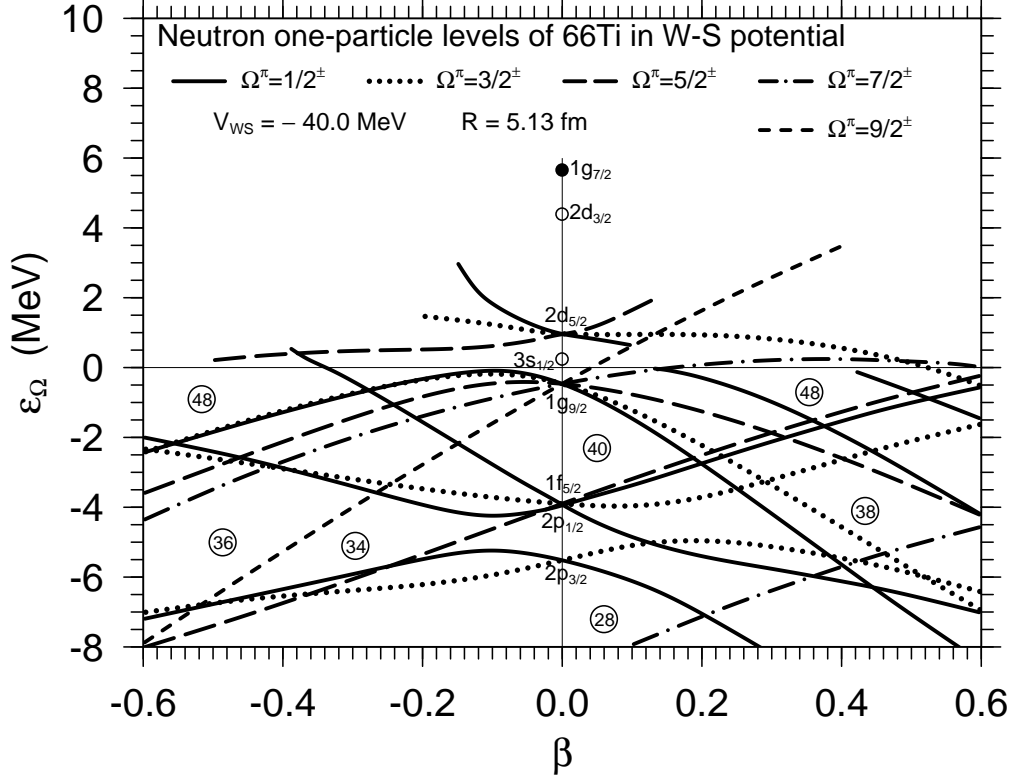


Fig. 9: Calculated neutron one-particle energies as a function of axially-symmetric quadrupole deformation. Parameters of the Woods-Saxon potential are chosen for the nucleus  ${}^{66}_{22}\text{Ti}_{44}$ . Bound one-particle energies at  $\beta = 0$  are  $-8.82$ ,  $-5.54$ ,  $-3.99$ ,  $-3.94$ , and  $-0.48$  MeV for the  $1f_{7/2}$ ,  $2p_{3/2}$ ,  $2p_{1/2}$ ,  $1f_{5/2}$ , and  $1g_{9/2}$  levels, respectively, while one-particle resonant  $2d_{5/2}$ ,  $1g_{7/2}$ , and  $1h_{11/2}$  levels are obtained at  $+0.96$ ,  $+5.66$ , and  $+7.57$  MeV, respectively. The  $2d_{3/2}$  one-particle resonant level is not obtained for the present potential, however, its approximate position at  $\beta = 0$  is denoted by an open circle, at which an eigenphase does not reach, but comes close to  $\pi/2$ . The  $3s_{1/2}$  resonant level does not exist in any case, but the open circle at  $\beta = 0$  indicates the energy obtained by extrapolating the solid curve of the bound  $\Omega^\pi = 1/2^+$  orbit for  $\beta > 0.12$  to  $\beta = 0$ , although the calculated solid curve reaches 0 at  $\beta = 0.12$  and cannot continue to  $\beta < 0.12$ . The major component of the solid curve for  $\varepsilon_\Omega(< 0) \rightarrow 0$  is clearly  $3s_{1/2}$ . One-particle resonant levels for  $\beta \neq 0$  are not plotted if they are not relevant for the present discussion. The neutron numbers, 28, 34, 36, 38, 40 and 48, which are obtained by filling all lower-lying levels, are indicated with open circles. One-particle levels with  $\Omega = 1/2, 3/2, 5/2, 7/2$  and  $9/2$  are expressed by solid, dotted, long-dashed, dot-dashed, and short-dashed curves, respectively, for both positive and negative parities.